# A Fast Pulsed Neutron Source Driven by a Pulsed Current Transformer

M. Krishnan[1], B. Bures[1], J. Thompson[2], R. Madden[1] and F. Blobner[1]

[1] Alameda Applied Sciences Corporation, San Leandro, CA, USA
[2] Consultant, San Diego, CA, USA

Email contact of main author: krishnan@aasc.net

**Abstract**. Pulsed neutron accelerators have been considered for active interrogation of special nuclear materials and also for location and imaging of explosives using PFNA. Alameda Applied Sciences Corporation is developing a <40ns pulsed neutron source for these applications, based on the dense plasma focus (DPF). The DPF benefits from well established scaling laws that cover a wide range of outputs from $10^4$ up to $10^{12}$ n/pulse. The strong scaling of neutron output with discharge current (as the fourth power of the current) and the fact that the voltage required is relatively low (~10kV for a small source), allows the use of a pulsed current transformer architecture to efficiently drive the DPF. This paper describes the performance of a unit module of such a transformer driven neutron source. A single Thyratron switch is used to transform a 27kV/11kA pulse on the primary side of a metglas transformer into a 9kV/33kA pulse on the secondary. This secondary pulse drives a DPF at rep-rates from 10-100Hz, to produce ~20ns neutron pulses. Optimization of the DPF head and its electrical coupling efficiency to the transformer driver are discussed. Conceptual designs for 100kA and 300kA versions of the pulsed transformer are presented, that are capable of driving DPF sources to $10^{12}$ n/s (DT) output with 14.1MeV neutrons in <40ns pulse widths.

## 1 Introduction

Rapid detection of special nuclear materials (SNM) is a critical problem for many countries. The problem includes quasi-static targets in well-defined situations, such as cargo containers passing through defined portals. The science and technology of special nuclear material (SNM) detection are well documented, but detailed threat profiles, capability of deployed systems and scientific data for specific threat profiles are seldom discussed [1]. It is impractical to detect SNM by passive means, simply because these emissions are easy to shield. There are two major active interrogation approaches: one uses an intense photon source to induce fission in the SNM and detect the subsequent gamma and neutron emissions; another uses a source of neutrons to achieve the same result. One potential advantage of neutrons is the ability to also detect high explosive (HE) and illicit drugs. Despite the demonstrated success of active neutron and photon interrogation methods, new radiation sources are required to improve the performance of existing detection systems. There is interest in neutron sources that possess the following characteristics: $>10^8$ n/s, short pulse width, sharp pulse cut-off, and operation between 10Hz and 2000Hz. Almost half of all the causalities in the Iraq war have been caused by improvised explosive devices (IEDs) [2]. The US Department of Homeland Security has been working since its inception on detection of explosives in luggage and cargo. With widely varied environments for the IED problem (3D environment full of debris, day-to-day items, people, plants and animals), one has to address buried and camouflaged IEDs. There is a premium on deployment of a detection system that can locate IEDs from sufficiently far away in a moving vehicle, so that convoys can avoid or deactivate the IED without loss of life.

Over the years, several approaches have been proposed to detect explosives in IEDs and buried landmines, including laser based systems, acoustic systems, chemical “sniffers” and neutron probes. Neutron probes are particularly useful as they induce characteristic gamma emissions from the constituent atoms of the hidden threat, which may be rapidly analyzed to obtain a signature of IEDs. However, whereas it is possible with today’s technology to produce 2D resolution in spherical coordinates ($\theta$ and $\Phi$) of the gamma radiation from the

hidden explosive, it is much harder to pinpoint its radial distance from the detector and source. This third and critical dimension is possible to pinpoint if one uses a very fast pulsed neutron source and time-of-flight range gating techniques. For example, a 5ns neutron pulse from a DT reaction (~14MeV) would provide ~25cm spatial resolution, to complement the 2D (θ & Φ) information from a gamma camera, allowing precise location and avoidance of the IED from a moving vehicle.

AASC's is developing a fast pulsed, dense plasma focus (DPF) source to produce ~10ns neutron pulse width at a neutron rate that meets detector requirements for both SNM and IED detection. Our breadboard DPF has demonstrated the ability to reliably produce narrow pulses in time (<20ns) and energy (2.45±0.1MeV for DD) with intense radiation bursts. This type of DPF source has evolved over 40 years of prior research, mostly in University and National Laboratory settings. Single-shot neutron outputs from $10^4$n/p (DD) up to $10^{12}$n/p (DD) have been demonstrated at pinch plasma currents from ~50kA up to 1.5MA [3]. Measured neutron pulse widths range from ~10ns in <300kA machines up to 70ns for the highest current experiments (>1MA). The inherent scalability of the DPF allows us to envision larger, higher powered versions of our DPF that may produce up to $10^{10}$n/s (DD) in a vehicle-mountable configuration. The DPF as a soft x-ray/extreme ultraviolet (EUV) source has been quasi-commercially developed for two applications: a Ne soft x-ray source (~1nm) for proximity x-ray lithography [4], operating with ~1kJ stored at ~20Hz and a Xe EUV source [5] (~13nm) with ~2J stored at up to 2kHz. These prior demonstrations show that the DPF neutron source proposed by AASC is capable of operation at up to 1 kHz, if a solid state switched pulsed power system is built. Recently we have developed an innovative concept for delivering high currents to DPFs at lower stored energy than before. This innovative concept is described in this paper.

## 2 Design considerations

The design of the transformer driver for the DPF is specified by starting at the load end and working backwards. Figure 1a shows the typical DPF operation with the current sheet shown at different times, from initial breakdown along the insulator, to coaxial acceleration and finally the radial implosion to form a tight pinch.

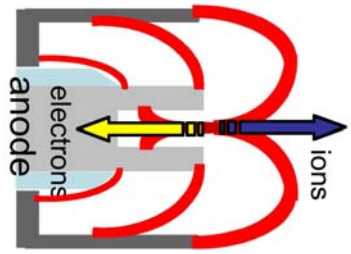


Fig.1a: The DPF current sheet at: breakdown, coaxial acceleration and radial collapse into a pinch

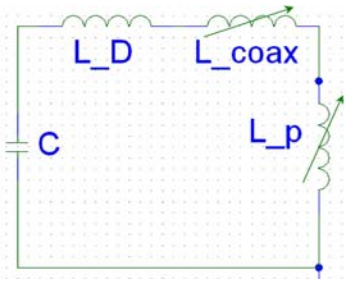


Fig.1b: Equivalent electrical circuit of the DPF

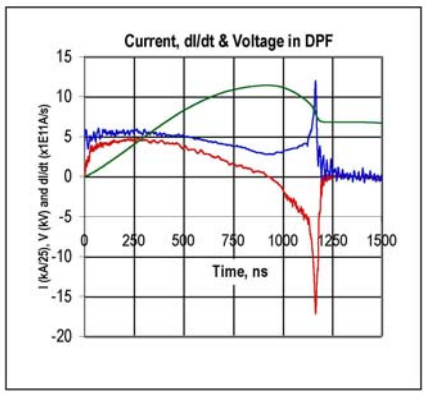


Fig.1c: Typical current (green), dI/dt (red) and voltage (blue) in a 300kA DPF

Figure 1b shows the electrical equivalent circuit. This RLC circuit consists of a capacitance C and driver inductance $L_D$, along with the time-varying inductance $L_{coax}$ due to the axial run-down of the current sheet, plus a (more rapidly varying) inductance $L_p$ for the radial pinch phase. Figure 1c shows representative current and voltage pulses from such a circuit. During the coaxial run-down phase of the DPF, the current builds up in the coaxial inductance and is

designed to reach a peak when the sheet reaches the open end of the electrodes. This coaxial phase is relatively slow, of ~1μs in most DPFs. When the sheet turns radially inwards and implodes in ~50-100ns, the rapidly increasing inductance $L_p$ reduces the current as shown and a "back emf" voltage, d/dt(LI), is generated. The sharp reduction in current is indicated by the d/dt(I) trace also shown in the figure.

Simple flux conservation and energy balance may be used to show that, when the peak current occurs at zero voltage on the capacitor, the current at pinch time is related to the peak current by:

$$\frac{I_p}{I_{peak}} = \frac{L_D + L_{coax}}{L_p + L_D + L_{coax}} \tag{1}$$

The fraction of energy extracted from the magnetic energy in the circuit is:

$$\frac{E_p}{E_o} = \frac{L_p}{L_p + L_D + L_{coax}} \tag{2}$$

It is well known [6] that neutron production in DPF pinches is driven by a beam-target process in which an energetic ion ($D^+$ or $T^+$) collides with dense regions of the pinch plasma to drive fusion more efficiently than is possible in the relatively cold (~1keV) plasma itself. Typical estimates of the $D^+$ beam energy are ~0.05-1MeV in high current DPFs. The source of such highly energetic ion beams is the spike in voltage d/dt(LI) due to the rapid increase in inductance of the radially collapsing pinch. This voltage spike can be »the ~10-30kV capacitor voltage of most DPFs. If the pinch collapses into a number of dense spots with low density gaps in between [7], a series of diodes is created, in which energetic ion and electron beams are generated (see Fig. 1a). The current in such beams is a small fraction of the pinch current and the net accelerating potential is some multiple of the capacitor voltage. It may be shown that the power in the driving ion beam is at a maximum when $L_p$ equals ($L_{coax}$+$L_D$). This is analogous to the Thevenin power transfer theorem for linear circuits.

To illustrate these arguments, consider a typical coaxial run-down inductance of say, 5nH and a vacuum feed inductance (including the insulator) of another 3nH. For a typical sinusoidal 300kA current rise-time of 1μs, the LdI/dt voltage required to drive 8nH is ≈4kV. The DPF head for a 300kA pinch might have a 30mm dia. anode coaxial with a 60mm dia. cathode. If the pinch dia. and length are 0.5mm and 10mm respectively, then the pinch inductance is ≈10nH. To maximize the power transfer to the pinch, we are left with a total inductance budget of only 2nH for the 300kA driver bank. The voltage required to charge the 10nH to peak current would be ≈5kV. Most DPF designs use much higher bank voltages.

The next constraint is the requirement for a rep-rate of ~100-1000Hz, to achieve adequate detection times in the field. This implies use of either Thyratrons or solid-state switches. The high current makes solid-state switches an expensive solution, but one that would offer the highest life-time. Thyratrons are a good compromise between cost and reliability. But typical Thyratrons operate best when switching <15kA, hence a 300kA neutron source would require >20 Thyratrons. Thyratrons operate well at voltages of up to 45kV. However, the DPF (as shown above) requires only ≈5kV to drive the pinch. It is obvious that by using a step-down transformer, we may reduce the voltage and increase the current from a Thyratron, to match more efficiently to a DPF. ***This is the basis for our approach***. A 300kA direct drive design (to generate $10^{10}$n/pulse DD or $10^{12}$n/s DT) would require 24 switches at a minimum. If the switch has a $10^8$ pulse lifetime under these conditions, that corresponds to 280 hours of continuous operation at 100Hz. If the detection system were used for 8 hours/week in the field, the switches would last about 35 weeks. The replacement cost of 24 switches every 9 months (~$100k) could be prohibitive. On the other hand, a lower voltage but higher current switch would be better. But the only switches that meet this criterion are large spark-gaps or

rail switches, which do not operate reliably (if at all) at >10Hz. But what if we were to insert a transformer into the circuit, so that the 36kV/13kA Thyratron looks (on the secondary side of a 4:1 step-down transformer) like a 9kV/52kA switch? Then the 300kA design would require only 6 Thyratrons. The replacement cost has been reduced by 4×, to ~$25k. An added advantage of the transformer architecture is that the static inductance of the driver is reduced (as seen by the DPF pinch load on the secondary side) by a factor of 16. This in turn reduces the stored energy required for a given current by 2×, as outlined below. Such a 2× reduction is crucial, as power is always at a premium in moving vehicles.

Consider a primary circuit with 7 Thyratron switches, each carrying 12kA at 33kV. The maximum Thyratron voltage and current are 44kV and 17kA, so we have allowed a safety factor of >25% in our design. If this primary driver is coupled to the DPF via a 4:1 step-down transformer, the secondary loop will have a voltage of ≈8kV and a current of 336kA. The 8kV/336kA secondary output meets the criteria defined above. *But there is a singular advantage to the transformation*. Suppose that the primary side inductance is 20nH (we will show why below). The secondary inductance is 16× lower, or only 1.6nH. This very low static inductance (as seen by the DPF load on the secondary side) meets the 2nH budget derived above, for maximum power transfer to the pinch. The next section describes the transformer driver architecture in greater detail.

## 3 Modular Thyratron Driver: Unit Module

Figures 1 and 2 show a photograph and inner details of the unit module of our transformer driver, which in this case was built as a 3:1 step-down transformer, just to test the concept.

Figure 1: Photograph of 3:1 step-down unit module Thyratron/transformer driver

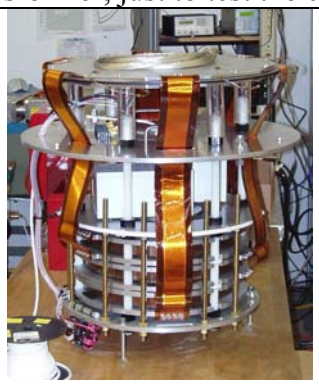

Figure 2: Interior details of 3:1 step-down transformer driver

The unit is contained in a 30-gallon oil drum, with the DPF mounted about 200mm above the driver as shown. The power is connected to the DPF via six sets of Cu strip-lines with Kapton insulation. We have developed a unit design for a Thyratron driven DPF geometry which consists of a Thyratron, multiple metglas cores, energy storage capacitors and an output stripline. Figure 2 shows the inner details of the driver tested. The primary current path is from the capacitors down the primary conduction posts, across the plate to the Thyratron and up the Thyratron back to the capacitors. The secondaries were formed by plates and tubes around each of the metglas cores. Six unipolar stripines (shown) provide an output from the module with an arrangement of 2 per secondary. Overall dimensions are approximately 500mm OD, and 400mm high. The secondaries as shown can provide pulses with a quarter-cycle time of up to 600 ns without reset current and up to 1μs with reset current.

### 3.1 Short Circuit and DPF Load Tests

Figure 3 shows measured current into a short circuit load (blue trace) and an analytical simulation of this current, assuming a linear, RLC circuit (red trace). The voltage on the primary was 14kV, which implies 4.667kV on the secondary.

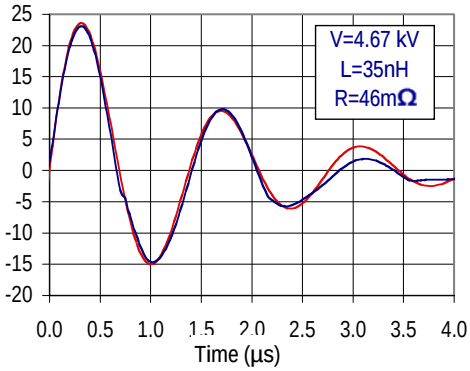


Figure 3: Measured shorts circuit current from unit module Thyratron Transformer driver (blue trace) and analytical current (red trace).

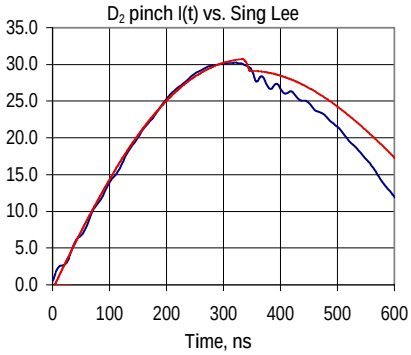


Figure 4: Measured current into a DPF load (blue trace) and simulated current (red trace) using S. Lee code [8].

The match between the simulation and the data is quite good in the first full cycle of the ringing waveform. The simulation deduced L=35nH and R=46mΩ on the secondary side of the transformer driver. With a 3:1 step-down ratio, these numbers would correspond to L=315nH and R=414mΩ on the primary side of the circuit. Each of the two 75nF/50kV capacitors was measured to have an ESR at this frequency of 0.8Ω, hence most of the resistance in the loop is from the (surprisingly dissipative) capacitors. The ringing which damps in the first half-cycle, is re-stimulated by the reverse conduction process of the Thyratron on the negative peak. The DPF neutron output occurs after a quarter cycle, so the reverse conduction is required (and successfully demonstrated here) because we need reverse conduction to get the full multi-year life from the Thyratron. The short circuit current of 23kA implies a current of 39.6kA at 24kV charge. With a more inductive DPF load, we expect closer to 30kA at 24kV. We next tested a DPF load, which consisted of a ≈3nH insulator, a 5.5mm diameter anode 15mm long and a 60mm diameter array of cathode rods. The DPF load hardware adds about 7nH of static, connection inductance to the circuit.

Figure 4 shows the current measured (blue trace) when the driver was connected to the DPF load. The peak current of 30kA is as expected. An excel macro written and refined over the years by S. Lee [8] was used to match (red trace) to the measured current. The inductance was assumed to be 43nH and the resistance 50mΩ, based on the shorts circuit analysis described earlier. For the given load geometry and operating conditions (pressure and charge voltage) The Lee code adjusts a few fitting parameters to get a close agreement to the measured current, including the d/dt(LI) dip. The fit is acceptable and provides a useful design tool with which to explore variations in the DPF load geometry. For example, the model suggests that a slightly longer anode at lower pressure would give higher neutron outputs. The unit module was fired at rep-rates of up to 100Hz under these conditions, to verify that the Thyratron/Transformer based approach was reliable at these rates.

### 3.2 Neutron Output

The unit module was run at 0.2Hz for 4311 pulses, to count neutron producing shots, using a BC400 scintillator/EMI 9813KB photomultiplier (PMT) detector. A typical current trace (blue) and PMT signal (green) are shown in Figure 5. The ~0.5-1V PMT signal corresponds to a sufficient flux of neutrons to give an analog current from the PMT. Hence the shape of

the PMT signal contains information about the time history of the neutron emission from the pinch.

Figure 6 plots a histogram of the number of events vs. pulse FWHM for the 4311 pulse run. As these were preliminary data from the unit module, the head has not yet been optimized. Hence only about 5% of all the pulses in this run made neutrons. The inset in figure 6 shows a magnified graph that indicates that for those few pulses that did make neutrons, the spread in FWHM is rather tight, 10±3ns. Such narrow pulses are very useful for range gating detection techniques. The speed of a 2.5MeV DD neutron is ≈2.2cm/ns. The 10ns FWHM pulse corresponds to a travel distance of ~22cm. With suitable detectors, it is hence possible to use time-of-flight gating to image SNM or HE with ~25cm spatial resolution. These pulse widths are to be contrasted with the typical ~1μs or longer pulses offered by today's commercially available neutron tubes.

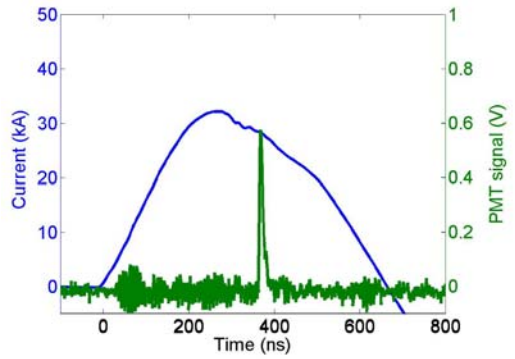


Figure 5: Measured DPF current at 24kV charge (blue trace) and PMT signal of neutrons (green trace).

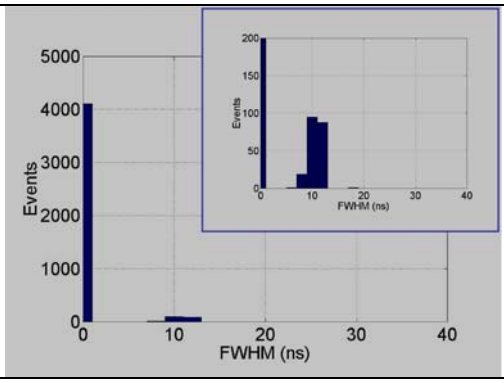


Figure 6: Histogram of neutron events from a 4311 pulse run at 0.2Hz. Inset shows a magnified histogram to reveal the narrow distribution of FWHM (≈10ns±3ns).

AASC operates three different DPF test-beds: DPF-1 is a 35-170kA/2Hz neutron source; DPF-3 is a 200-400kA/0.1Hz DPF, similar to one that was delivered to NTU/Singapore and dubbed NX-2 by the NTU group [9]. DPF-2 is the 100Hz unit module described earlier. DPF-1 has been operated in bursts of 300 pulses for >20,000 pulses. Under optimum conditions, the neutron output is reliable and reproducible to ±20%.

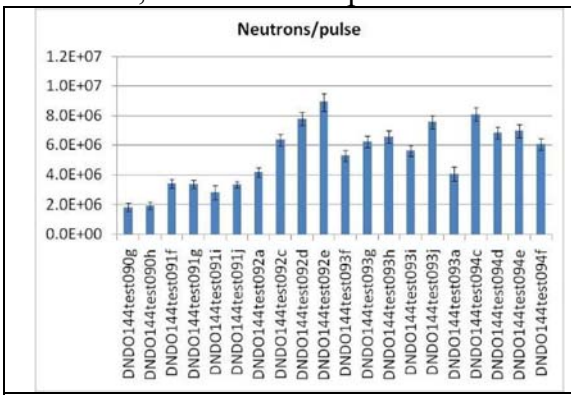


Figure 7: Histogram of neutron events from 100kA, 2Hz neutron source at AASC (DPF-1).

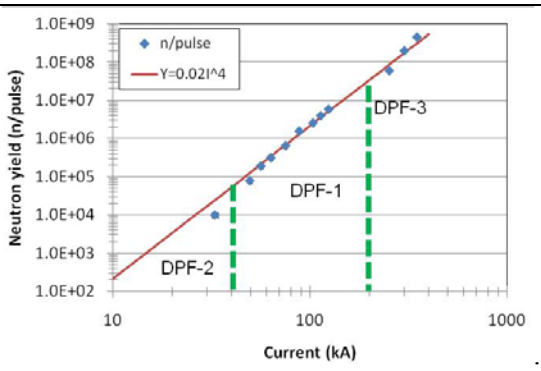


Figure 8: Scaling of DPF neutron output with peak current, from neutron sources, DPF-1, 2& 3.

An example of the output stability is shown in figure 7, which shows the variation in neutron output as measured over 20 consecutive, 300 pulse runs using DPF-1. Once the operating parameters were optimized, runs 8 through 20 show a mean output of $6.55\times10^6$ n/p with a mean standard deviation (1-σ) of 19%. This stability was achieved without gas flow or cooling. Prior work with Ne soft x-ray sources had shown that by adjusting the gas pressure (by a small flow) and cooling the electrodes, the output can be controlled to < ±20% over long (~5000 pulse runs). The data shown in Fig. 6 are the first data obtained from DPF-2. It is

anticipated that optimization of the electrodes and operating parameters will lead to similar output stability and reliability as has been measured in DPF-1.
Figure 8 shows how the neutron output scales with peak DPF current. The straight line (red) is the $I^4$ scaling law. These data verify the $I^4$ scaling over a wide range of currents. In particular, at 300kA, the measured output of ~$3\times10^8$ n/p implies a rate of $3\times10^{10}$ n/s at 100Hz when using a Thyratron/Transformer switched driver. With DT mixtures, the rate is projected to reach $10^{12}$ n/s. At 120kA, the rate would be ~$10^{10}$ n/s.
Figure 9 shows the PMT signal measured from DPF-1, to contrast with the pulse from DPF-2 shown in Figures 5 and 6.

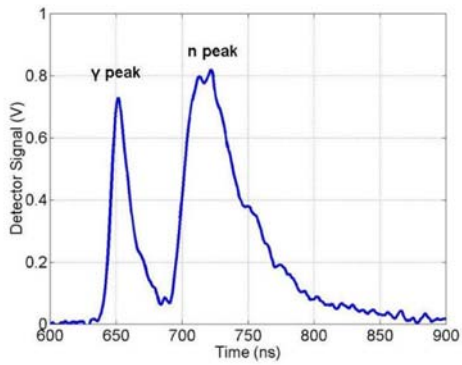


Figure 9: PMT signal showing hard x-ray peak followed by 2.45MeV neutron peak.

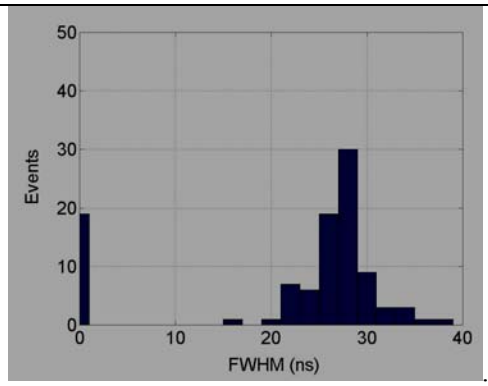


Figure 10: Histogram of neutron events from 100kA, 2Hz neutron source at AASC (DPF-1).

With reference to Fig. 1a, the energetic electron beam that is generated in the pinch produces bremsstrahlung from both the dense regions of plasma in the pinch as well as well by impinging upon the anode surface. The FWHM of this hard x-ray pulse is ~10ns and serves as a timing reference for time gating of neutron detectors. The delayed pulse in the figure is due to the slower 2.45MeV neutrons. In this case the FWHM of the neutron pulses is wider (27ns mean), as shown in Figure 8. A general trend has been observed that pulse width increases with current, because higher currents require larger anodes which then produce longer pinches that radiate for longer durations. One reason for longer pulses from longer pinches is that the pinch undergoes an elongation as the curved current sheet assembles. Such an elongation has been referred to as 'zippering' by analogy with the zipper in clothing. Zippering alone would broaden the neutron pulse width. But in addition, instabilities might also play a role. For example, the classical m=0 MHD instability would break the pinch up into a series of spots [7], each of which might radiate at slightly different times, leading to structure in and broadening of the pulse. Simulation and experiments are underway to understand the role that plasma instabilities and electrode shape might play in altering the dynamics of the assembly of the pinch on axis and hence the neutron pulse width. The goal is to reduce the pulse width so that more accurate range-gating detection concepts might be demonstrated at higher neutron rates in the future. Still narrower pulses would allow voxel maps of SNM or HE volumes to be created using space and time resolved detection.

## 4 Conceptual Designs of higher intensity neutron sources

Based on the unit module results, we have produced conceptual designs of higher output sources that could produce up to $10^{10}$ n/s (at 120kA) and $10^{12}$n/s (at 320kA) in DT mixtures. Figures 9 and 10 show our conceptual designs.
The dimensions of the 320kA unit will be approximately 1.65m diameter x 450mm high. These dimensions correspond to a total volume of ≈1 cubic meter. Stripline feeds are shown running along the top of the module in figure 10. The size and volume of the source make it

portable on an armored vehicle. The 83kW power requirement is also compatible with burst mode power derived from the vehicle's drive train with suitable power modulation.

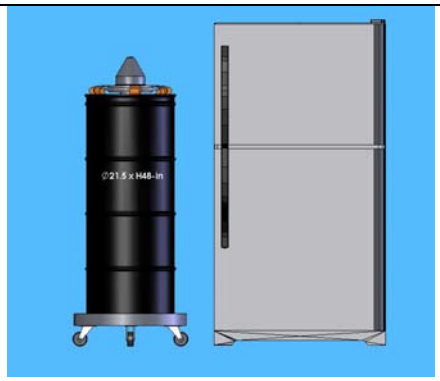

Figure 9 Artist's rendition of 120kA current transformer driven, $10^{10}$ n/s DT source

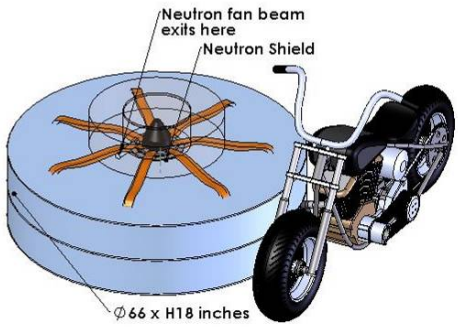


Figure 10: Artist's rendition of 320kA current transformer driven, $10^{12}$ n/s DT source .

## 5 Summary

This paper has described a Thyratron switched, step-down transformer design to provide higher efficiency drivers to Dense Plasma Focus neutron sources.. A unit module of the design was shown to operate reliably at up to 100Hz rep-rates, into shorts circuit and DPF loads. Preliminary measurements of neutron output show that this unit module follows the $I^4$scaling relation validated by us at 30-300kA currents and by several others at still higher currents. A point design for a 320kA/100Hz source was described, that could provide up to $10^{12}$ n/s in DT mixtures. The ultra-fast neutron pulses emitted by the DPF (measured to be as fast narrow as 10ns) offer the potential to develop new classes of range-gated detectors that could use time-of-flight techniques to provide high resolution imaging of objects in the field.

## 6 Acknowledgements

This research is supported by the Domestic Nuclear Detection Office of the US DHS and by the US Air Force via SBIR contracts.

## 7 References

1. T. Peurrung and E. Smith "Short Course: Nuclear Science for Homeland Security" 2006 IEEE Nuclear Science Symposium & Medical Imaging Conference. San Diego, CA October 29, 2006.
2. http://icasualties.org/oif/
3. S. Lee, "Current and neutron scaling for megajoule plasma focus machines", Plasma Phys. Control. Fusion 50 (2008) 105005 (14pp), Online at stacks.iop.org/PPCF/50/105005
4. R.R. Prasad, et al., "Neon dense plasma focus point x-ray source for ≤25 µm lithography", Proc. SPIE **2194**, 120 (1994
5. Akins, Robert P., Sandstrom, Richard L., Partlo, William N., Fomenkov, Igor V. High repetition rate laser produced plasma EUV light source, United States Patent 7361918, April 22, 2008
6. K. N. Koshelev and N. Pereira, "Plasma points and radiative collapse in vacuum sparks", J. Appl. Phys. 69 (IO), 15 May 1991
7. W Kies, B Lucas, P Rowekamp, F Schmitz, G Ziethen and G Decker, Plasma Sources Sci. Technol. 7 (1998) 21–27. Printed in the UKLee S Radiative Dense Plasma Focus Computation Package: RADPF http://www.intimal.edu.my/school/fas/ UFLF/
8. J. M. Koh R. S. Rawat, A. Patran, T. Zhang, D. Wong, S. V. Springham, T. L. Tan, S. Lee and P. Lee "Optimization of the high pressure operation regime for enhanced neutron output in a plasma focus device" *Plasma Sources Sci. Technol.* **14** (2005) 12–18.